Coordinate Sizing and Control of the Onboard Pulse Power Supply System

Wenjie Ao, *Graduate Student Member, IEEE*, Jiawei Chen, *Senior Member, IEEE*, and Wenjie Lv

***Abstract*—Onboard pulse power load features a high peak-to-average ratio, which would significantly impact the stable operation of the power supply system (PSS). Specifically, the supply voltage may reduce dramatically and eventually trigger system protection, thus sacrificing reliability. One effective way to address this issue is to connect an active capacitor, which is defined as a capacitor with a bidirectional dc/dc converter, to the power supply's output. However, as the active capacitor is usually used to accommodate all the pulsed load with the conventional control schemes, the power supply's specific power would be limited due to the less optimized system's volume, making its implementation constrained. In this article, a coordinate sizing strategy is first proposed. The system's volume is minimized by using the battery to supply a portion of the pulsed load. Afterward, a simple pulsed current reference generation method is proposed for the active capacitor. The pulse power tracking performance is further improved. A prototype of a pulse PSS with 2.7-kW constant power and 30-kW peak power is designed in the lab. The experimental results verify the validity of the proposed method.**

***Index Terms*—Active capacitor, coordinate sizing, low pulsating frequency, pulse current extraction, pulse power supply.**

I. Introduction

In RECENT years, more-electric and all-electric technology has rapidly developed in the transportation industry, such as more-electric aircraft [1], [2], [3], more-electric ships [4], [5], [6], etc. Electric loads with pulse power characteristics, such as radar, electromagnetic weapons, and electric actuation systems, are increasingly equipped onboard the transportation electrification systems. Typically, these loads have high peak-to-average ratios and low and variable pulsating frequencies [7], [8], seriously affecting the power quality and system reliability of the power supply system (PSS).

Generally, onboard electrical loads are powered by a single power supply source, such as a generator or a battery [9], [10]. In order to improve energy utilization efficiency, reduce environmental pollution, and make full use of the characteristics of different power sources, many hybrid power supply systems (HPSSs) have been proposed recently, such as fuel cell-battery HPSS [11], [12], fuel cell-battery-supercapacitor HPSS [13], diesel generator-battery HPSS [14], [15], etc. The existing HPSS usually consists of at least one primary power supply and one auxiliary power supply (usually an energy storage unit (ESU)) to cope with increasingly complex power scenarios. In case of pulsed load power, as the dynamics and peak power of the main power supply do not well fit the dynamics of the pulsed loads, the output voltage of the PSS would reduce dramatically, making the PSS more likely to be shut down. To address this issue, an ESU like a battery or a sizeable electrolytic capacitor with fast dynamics can be connected to the output of the PSS, forming a pulsed PSS (PPSS). The ESU of the PPSS is then controlled to pick up the pulsed part and leave the average load power to the main power supply. By applying such a decoupled power regulation, the output voltage of the PPSS can be made relatively stable during the pulsating period. So far, the most commonly used decoupling power regulation techniques can be categorized into passive decoupling [16], [17], [18] and active decoupling [7], [8], [19], [20], [21], [22], [23], [24], as shown in Fig. 1. Although the former is simple to implement, its applications in aeronautics and aerospace are not desired due to the requirement of using bulky ESUs, as seen in Fig. 1(a). Contrarily, the active power decoupling control is more promising. When capacitors are adopted as ESU, by adding dc/dc conversion units between

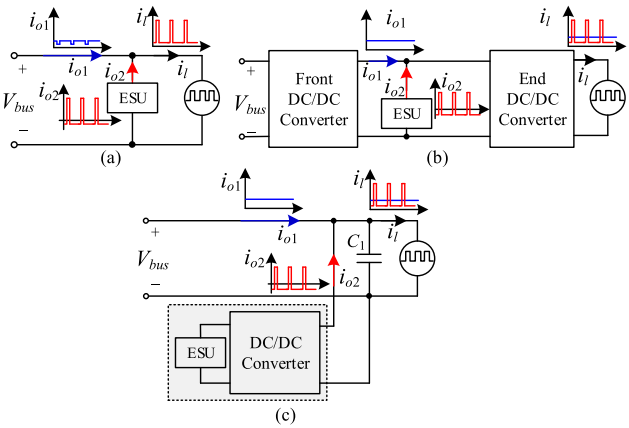

Fig. 1. Power decoupling schemes for PPS.

Manuscript received 23 November 2022; revised 30 May 2023 and 8 August 2023; accepted 15 September 2023. Date of publication 5 October 2023; date of current version 13 April 2024. This work was supported by the National Natural Science Foundation of China under Grant 51877019 and Grant 52377190. *(Corresponding author: Jiawei Chen.)*

The authors are with the College of Automation, Chongqing University, Chongqing 401331, China (e-mail: wenjieao@cqu.edu.cn; echenjw@cqu.edu.cn; 202213131079t@stu.cqu.edu.cn).

Color versions of one or more figures in this article are available at https://doi.org/10.1109/TIE.2023.3319722.

Digital Object Identifier 10.1109/TIE.2023.3319722

0278-0046 © 2023 IEEE. Personal use is permitted, but republication/redistribution requires IEEE permission.
See https://www.ieee.org/publications/rights/index.html for more information.

Authorized licensed use limited to: CHONGQING UNIVERSITY. Downloaded on March 07,2026 at 09:05:34 UTC from IEEE Xplore. Restrictions apply.

the capacitor terminal and the output of the main power supply, the voltage variation range of the decoupling capacitor can be enlarged. Eventually, the capacitor used for power decoupling can be made very small, and the specific power of the PPSS can be highly increased. Currently, there are two commonly used active decoupling control strategies, namely series decoupling [7], [8], [19] and parallel decoupling [20], [21], [22], [23], [24], as depicted in Fig. 1(b) and (c), respectively. Although the PPSS with the series decoupling strategy features a higher conversion efficiency, it requires two dc/dc conversion stages, which raises costs and reduces reliability. Meanwhile, the parallel decoupling strategy, shown in Fig. 1(c), is widely used in real applications as only a bidirectional dc/dc converter is needed, making the system cost-effective and helpful for increasing the system's specific power; in addition, it can be more easily integrated into the existing PSS. In the rest of this article, the decoupling structure composed of a capacitor with a bidirectional dc/dc converter is called an active capacitor.

So far, many researchers have studied the active capacitor's control architecture, operational principle, and design details. Since the main power supplies in electric ships, electric vehicles, and large aircraft are usually generators mounted with the engine, the active capacitors in these applications are only controlled to absorb the pulsating power [25], [26], [27]. Therefore, the size and weight of the PPSS are somewhat determined after the load profile is set. However, for some special applications, such as rockets and missiles, the main power supply only needs to supply load power for several minutes. Therefore, a small battery pack other than a generator is usually used as the main power supply. In this case, the volume and weight of the PPSS will be highly influenced by the distribution manner of the pulsed power between the main power supply and the active capacitor. Thus, coordinate sizing should be made further to reduce the volume and weight of the PPSS.

The optimal sizing methods for different energy resources in a PSS are mainly classified into statistical and search methods. The statistical method is not very sensitive to parameter variations [28]. While the search method [29], [30], such as particle swarm optimization, usually cannot guarantee obtaining the global optimal solution. In addition, most available methods are targeted at minimizing the cost and maximizing the profit [31], [32], [33]. None of them aimed at maximizing the system power density or minimizing the system volume and weight. Apart from that, since there are many system constraints, such as the finite capacity of the main power supply (i.e., battery), the low- and variable-frequency of the pulsed load power, and the requirement of absorbing regenerative energy, the solution to the optimization problem is quite complicated.

Besides, it is known from the research results that the output current of the active capacitor should be controlled to follow the pulsating load current closely in order to achieve power decoupling. However, because the pulsating component of the load current, which is used as the current reference of the active capacitor, is conventionally extracted from the load current by using a high-pass filter (HPF) [21], the pulsating current reference signal is not well suited for transient processes when the frequency of the pulsed load is low and variable. As a result, the current tracking performance of the active capacitor, and then the performance of the PPSS, has deteriorated.

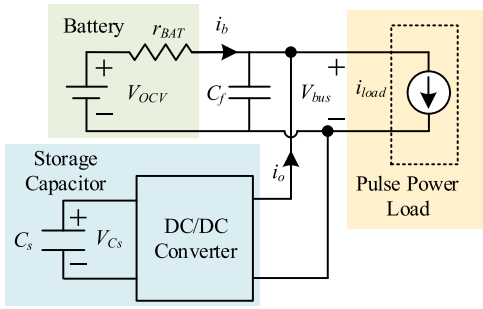

Fig. 2. Battery-active capacitor converter PPSS.

This article aims to solve the optimal sizing and control problem of the onboard PPSS. The intended contributions of this article include the following conditions:

1) A simple analytical method based optimal sizing method, which is targeted at minimizing the volume of the PPSS under various system constraints, especially the distribution manner of the pulsed power between the main power supply and the active capacitor, is proposed. The system's specific power can be improved.
2) A high-performance pulse current reference extracting method is proposed. The undesirable current reference signal under low and variable frequency caused by the HPF in the transient process is solved.

The rest of the article is organized as follows. In Section II, the system architecture under consideration is given. The characteristics of the pulsed power load are also briefly provided. The coordinate sizing method of the PPSS, which considers all the operational constraints, is proposed in Section III. Section IV elaborates on the pulse current reference-extracting method. In Section V, an example PPSS is designed, and experiments are done to verify the validity of the proposed methods. Finally, Section VI concludes this article.

II. System Description

Fig. 2 shows the architecture of the considered PPSS composed of a battery (i.e., the main power supply) and an active capacitor formed by a storage capacitor C_s and a bidirectional dc/dc converter. This PPSS is widely used in a rocket to supply power to the radar, rudder adjustment system, and electric valve control system, which have pulsed power characteristics. A filter capacitor C_f is also connected to the dc bus to supply part of the pulse power in the transient process. In Fig. 2, V_{OCV} is the battery open-circuit voltage, i_b stands for the battery output current, r_{BAT} is the battery internal resistance, i_{load} represents the load current, i_o is the output current of the active capacitor converter, and V_{Cs} is the voltage of the capacitor C_s.

Fig. 3 shows the typical pulsed load profile of the rocket. Its peak and constant currents are 120 and 10 A, respectively. The pulsating frequency ranges from 0.2 to 5 Hz, and the pulsewidth varies between 20 and 50 ms. When the pulse ends, regenerative energy immediately generates and feeds back to the dc bus for

Authorized licensed use limited to: CHONGQING UNIVERSITY. Downloaded on March 07,2026 at 09:05:34 UTC from IEEE Xplore. Restrictions apply.

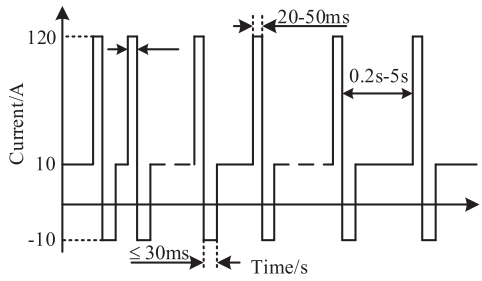

Fig. 3. Typical load profile of the considered load in a rocket.

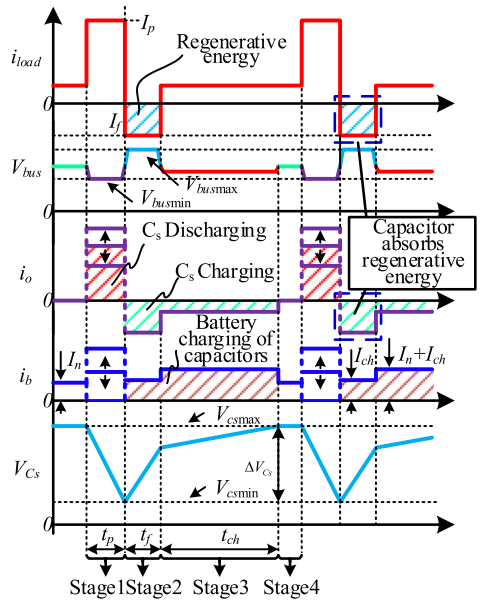

Fig. 4. Key operational waveforms of PPSS.

30 ms, with a regenerative pulse current being less than 30% of the peak current.

The considered PPSS have four typical operation stages, as shown in Fig. 4. Detailed operation stages are discussed in the following.

Stage 1: The pulse operation stage. The active capacitor and the battery work together to power the pulsed load. Notably, the battery also needs to supply some portion of the pulsed power at this stage. The percentage of the load power it needs to supply will be determined by the coordinate sizing method proposed in this article.

Stage 2: The energy regeneration stage. Once the pulsed load ends, the regenerative energy generates, which is caused by the braking of the servo system. The regenerative energy should all be absorbed by the active capacitor.

Stage 3: Capacitor charging stage. The battery would provide the needed constant load power. Meanwhile, it keeps charging the storage capacitor C_s until it is fully charged and its terminal voltage reaches the maximum value.

Stage 4: Pulse preparation stage. The battery keeps providing the needed constant load power. At the same time, the active capacitor stops working as it is fully charged. The system gets ready to provide the pulsed load power for the next round.

III. Coordinate Sizing of the PPSS

A. Optimization Objective

Since the primary optimization goal is to increase the specific power of the PPSS, the system volume (or weight) is chosen as the optimization index.

It should be noted that the energy stored in the battery is fixed because the rocket only needs to operate for a few minutes in the launching process. In addition, the stored energy keeps decreasing with load consumption. Therefore, the battery and the active capacitor (including the storage capacitor and the dc/dc converter) make up most of the system's volume. Hence, the objective function can be determined as

$$\min J = \min(\mathrm{Vol}_{\mathrm{BAT}} + \mathrm{Vol}_C + \mathrm{Vol}_{\mathrm{CTRL}}) \tag{1}$$

where $\mathrm{Vol}_{\mathrm{BAT}}$, Vol_C, and $\mathrm{Vol}_{\mathrm{CTRL}}$ are the volume of the battery, storage capacitor, and dc/dc converter, respectively.

Because the battery pack is usually composed of many standard cells connected in series and parallel, the total volume of the battery pack can be expressed as

$$\mathrm{Vol}_{\mathrm{BAT}} = k_{\mathrm{BAT}} Q_{\mathrm{BAT}} V_{\mathrm{BAT}} \tag{2}$$

where Q_{BAT} is the battery's capacity and k_{BAT} is a constant related to cell types.

Similarly, the total volume of the storage capacitor of the active capacitor unit can be expressed as

$$\mathrm{Vol}_C = k_C(V_C) Q_C \tag{3}$$

where V_C and Q_C are the terminal voltage and capacity of the storage capacitor, respectively, and k_C is a constant related to the capacitor type and its terminal voltage.

As for the dc/dc converter, on the one hand, because the fuselage of the rocket is mainly used as the heat sink of the dc/dc converter, its volume is mainly determined by the volume of the PCB, inductor, power switches, and control board, which are all closely related to the power rating of the converter. On the other hand, although some of the pulsed load power would be absorbed by the battery, most of the pulsed power is still provided by the active capacitor. In this case, the volume of the dc/dc converter is mainly determined by the peak load power, which is a determined value after the load profile is set. Therefore, it is reasonable to assume the volume of the dc/dc converter to be a fixed value for simplicity in this article.

B. Operation Constraints

1) Bus Voltage Constraints: In extreme circumstances, the bus voltage should also be kept within a specific range to guarantee the pulse load's expected performance. According to Fig. 2, the bus voltage, which is the battery's output voltage, can be expressed as

$$V_{\mathrm{bus}} = V_{\mathrm{OCV}} - r_{\mathrm{BAT}} i_b \tag{4}$$

Authorized licensed use limited to: CHONGQING UNIVERSITY. Downloaded on March 07,2026 at 09:05:34 UTC from IEEE Xplore. Restrictions apply.

where V_{bus} is the bus voltage. Its variation during system operation should satisfy

$$V_{\text{bus min}} \le V_{\text{bus}} \le V_{\text{bus max}} \tag{5}$$

where V_{busmin} and V_{busmax} are the minimum and maximum allowable values of bus voltage, respectively.

2) Battery Constraints: Since the battery's energy is the total available energy of the PPSS, the battery's capacity should cover all of the needed energy. Therefore, we have

$$Q_{\text{BAT}} V_{\text{BAT}} \ge W_{\text{load}} - W_{\text{feb}k} + W_{\text{loss}} \tag{6}$$

where V_{BAT} is the nominal voltage of the battery; W_{load} is the energy consumed by the load; $W_{\text{feb}k}$ is the load regenerative energy, and W_{loss} is the total energy loss. W_{load} and $W_{\text{feb}k}$ can be calculated according to the pulsed load characteristics shown in Fig. 4. W_{loss} can be estimated using the converter efficiency and battery parameters.

3) Capacitor Charging Constraint: After the discharging cycle, the storage capacitor should be fully charged before the arrival of the next pulse. Hence, the capacitor charging current would satisfy

$$V_{\text{bus}} I_{\text{ch}}(t_{\text{ch}} + t_f) + V_{\text{bus}} I_f t_f \ge \frac{1}{2} Q_C V_{C\,\text{max}}^2 - \frac{1}{2} Q_C V_{C\,\text{min}}^2 \tag{7}$$

where I_{ch} is the battery's charging current to the capacitor; I_f is the regenerative current flow back to the active capacitor; and t_{ch} and t_f are the duration of I_{ch} and I_f, respectively.

C. Coordinate Sizing

As known in (2) and (3), the battery and storage capacitor volumes are proportional to their capacities. Thus, it is necessary to find the exact percentage of the pulsating load power that the battery and the active capacitor have to supply in order to achieve the coordinated sizing of the two power supplies. The sizing method can be deduced from the operation stages shown in Fig. 4.

In stage 1, the battery and the active capacitor work together to supply power to the load. Assuming that the pulsating power distribution ratio between the battery and the active capacitor are λ_{BAT} and λ_C, respectively, which satisfy $\lambda_{\text{BAT}} + \lambda_C = 1$ and $\lambda_{\text{BAT}}, \lambda_C \in (0,1)$. According to the load profile, the minimum capacity required by the storage capacitor C_s of the active capacitor unit can be derived as

$$Q_{Cs} = \frac{2 V_{\text{bus}} I_p t_p \lambda_C}{V_{Cs\,\text{max}}^2 - V_{Cs\,\text{min}}^2} \tag{8}$$

where I_p is the peak of the pulse current; t_p is the lasting time of the pulse peak; and $V_{Cs\text{max}}$ and $V_{Cs\text{min}}$ are the upper and lower limits of the capacitor voltage, respectively.

When ignoring the influences of temperature and state of charge, the internal resistance of the lithium battery, the nominal voltage, and the battery capacity satisfy [34]

$$r_{\text{BAT}} = k_r \frac{V_{\text{BAT}}}{Q_{\text{BAT}}} \tag{9}$$

where k_r is a constant related to the battery type.

Considering that the battery energy depletes continuously with time and it must be able to supply the required load power till the end of the last pulse. For power cells, when its open-circuit voltage is equal to the nominal voltage, we consider that the discharge performance at this time is not sufficient to support its continued operation. Thus, we chose V_{BAT} to calculate the minimum capacity of the battery. In this stage, the battery capacity should satisfy (10), which is obtained based on (4), (5), and (9)

$$Q_{\text{BAT}} \ge \frac{k_r V_{\text{BAT}} (1 - \lambda_C) I_p}{V_{\text{BAT}} - V_{\text{bus min}}}. \tag{10}$$

In stage 2, the battery and regenerative energy charges the storage capacitor C_s simultaneously. The battery's output current is less than that in stage 3. Hence, there is no need to consider the bus voltage constraint in this stage.

In stage 3, the battery supplies the needed constant load power and simultaneously charges the storage capacitor C_s. The battery's output current is then deduced as

$$i_b = I_{\text{ch}} + I_n \tag{11}$$

where I_n is the constant load power.

Combining (4), (5), (7), (8), (9), and (11), the minimum battery capacity can be deduced as

$$Q_{\text{BAT}} \ge \frac{[\lambda_C I_p t_p - I_f t_f + I_n (t_{\text{ch}} + t_f)] k_r V_{\text{BAT}}}{(t_{\text{ch}} + t_f)(V_{\text{BAT}} - V_{\text{bus min}})}. \tag{12}$$

In stage 4, as the battery's output current is less than or equal to that of stage 3, the battery's capacity has to satisfy (12) in stages 2 to 4.

Hence, (6), (10), and (12) together delimit the boundaries of selecting the battery's capacity, which is further defined as Q_{BAT1}, Q_{BAT2}, and Q_{BAT3}, respectively. That means, (6), (10), and (12) must be satisfied simultaneously.

Afterward, the minimum volume of the PPSS (Vol_{PPS}) can be obtained as

$$\text{Vol}_{\text{PPS}} \ge \max \left\{ \begin{array}{l} k_{\text{BAT}} Q_{\text{BAT1}} V_{\text{BAT}} + k_C(V_C) Q_{Cs} + \text{Vol}_{\text{CTRL}}, \\ k_{\text{BAT}} Q_{\text{BAT2}} V_{\text{BAT}} + k_C(V_C) Q_{Cs} + \text{Vol}_{\text{CTRL}}, \\ k_{\text{BAT}} Q_{\text{BAT3}} V_{\text{BAT}} + k_C(V_C) Q_{Cs} + \text{Vol}_{\text{CTRL}} \end{array} \right\}. \tag{13}$$

It is known from (13) that the part marked in red does not affect the optimization result because when comparing the size between these three values, the part marked in red cancels out during the comparison. Therefore, the system volume can be optimized once the optimum Q_{BAT} and λ_C are determined. Since Q_{BAT} is also a function of λ_C, the problem of optimization of PPSS's volume can be transformed into the problem of finding the optimum Q_{BAT} and λ_{C}.

By drawing the curves of $Q_{\text{BAT}i}$ with respect to λ_C under different load conditions and system constraints, four possible curve combinations can be generated with the movement of Q_{BAT1} (see Fig. 5), which is determined by total the energy required by the load and regardless of the varying of λ_C. The detailed analyzing process is provided in the Appendix, wherein the $Q_{\text{BAT}i}|_{\lambda C\,=\,0}$ and $Q_{\text{BAT}i}|_{\lambda C\,=\,1}$ are determined. Since the three inequalities in (6), (10), and (12) have to be satisfied

Authorized licensed use limited to: CHONGQING UNIVERSITY. Downloaded on March 07,2026 at 09:05:34 UTC from IEEE Xplore. Restrictions apply.

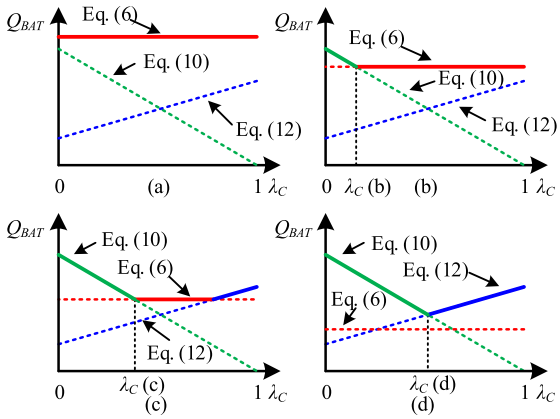

Fig. 5. Four possible cases of battery capacity boundary.

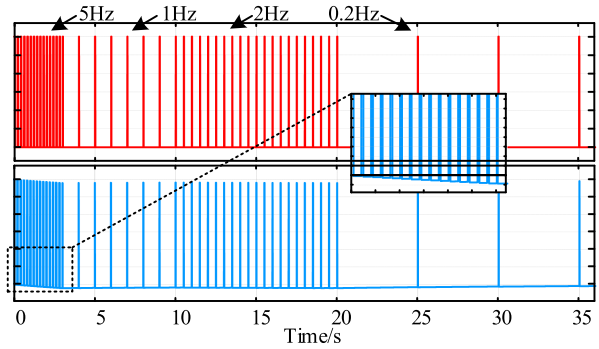

Fig. 6. Output current waveforms after HPF.

simultaneously, the solid lines lay out the boundaries of the selection of Q_{BAT}.

As shown in Fig. 5, four possible cases are considered, shown as follows:

Case 1: The value of Q_{BAT1} is greater than $Q_{\mathrm{BAT2}}|_{\lambda C\,=\,0}$ and $Q_{\mathrm{BAT3}}|_{\lambda C\,=\,1}$. In this case, the optimum battery capacity should be selected as Q_{BAT1}, which is irrelative to λ_C, as shown in Fig. 5(a). Alternatively, the active capacitor is not needed to guarantee the system's normal operation and satisfy the constraint of bus voltage. The optimal $\mathrm{Vol}_{\mathrm{PPS}}$ became

$$\mathrm{Vol}_{\mathrm{PPS}} = k_{\mathrm{BAT}} Q_{\mathrm{BAT1}}, \lambda_C \in (0,1). \tag{14}$$

Case 2 and Case 3: The value of Q_{BAT1} is smaller than $Q_{\mathrm{BAT2}}|_{\lambda C\,=\,0}$ and greater than $Q_{\mathrm{BAT3}}|_{\lambda C\,=\,1}$, as shown in Fig. 5(b), or the value of Q_{BAT1} is smaller than $Q_{\mathrm{BAT2}}|_{\lambda C\,=\,0}$ and $Q_{BAT3}|_{\lambda C\,=\,1}$, but greater than the cross-point of Q_{BAT2} and Q_{BAT3}, as shown in Fig. 5(c). In these two cases, the optimum battery capacity should also be selected as Q_{BAT1}. Combine (6) and (10), the optimum $\mathrm{Vol}_{\mathrm{PPS}}$ and the optimum λ_C become

$$\mathrm{Vol}_{\mathrm{PPS}} = k_{\mathrm{BAT}} Q_{\mathrm{BAT1}} V_{\mathrm{BAT}} + k_C(V_C) Q_{Cs} + \mathrm{Vol}_{\mathrm{CTRL}} \tag{15}$$

$$\lambda_C = \lambda_C(b) = \lambda_C(c) = 1 - Q_{\mathrm{BAT1}} \cdot \frac{V_{\mathrm{BAT}} - V_{\mathrm{bus\,min}}}{k_r V_{\mathrm{BAT}} I_p}. \tag{16}$$

Case 4: The value of Q_{BAT1} is smaller than $Q_{\mathrm{BAT2}}|_{\lambda C\,=\,0}$, $Q_{\mathrm{BAT3}}|_{\lambda C\,=\,1}$, and the cross-point of Q_{BAT2} and Q_{BAT3}, as shown in Fig. 5(d). In this case, the optimum battery capacity should be selected as the cross-point of Q_{BAT2} and Q_{BAT3}. Combine (10) and (12), the optimum $\mathrm{Vol}_{\mathrm{PPS}}$ and the optimal λ_C become

$$\mathrm{Vol}_{\mathrm{PPS}} = k_{\mathrm{BAT}} \frac{k_r V_{\mathrm{BAT}}[I_p t_{\mathrm{ch}} - I_f t_f + I_n(t_{\mathrm{ch}} + t_f)]}{(V_{\mathrm{BAT}} - V_{\mathrm{bus\,min}})(t_p + t_f + t_{\mathrm{ch}})} V_{\mathrm{BAT}} + k_C(V_C) Q_{Cs} + \mathrm{Vol}_{\mathrm{CTRL}} \tag{17}$$

$$\lambda_C = \lambda_C(d) = \frac{I_p(t_{\mathrm{ch}} + t_f) + I_f t_f - I_n(t_{\mathrm{ch}} + t_f)}{I_p(t_p + t_f + t_{\mathrm{ch}})}. \tag{18}$$

IV. Pulse Reference Extraction and Control for Active Capacitor

After determining the optimum pulse current distribution method λ_C according to (16) and (18), it is then to make the active capacitor provide this required part of the pulsed load current through its control system. That is, the output current of the active capacitor should be controlled to follow the current reference composed of pulsating component of load current and the optimum distribution mechanism λ_C. The control system proposed in [21] can be obtained to achieve this goal.

In [21], the pulsating component of the load current is extracted by filtering the load current using an HPF. However, when it is applied to low- and variable-frequency pulsed load situations, the fixed cutoff frequency filter is no longer applicable. Fig. 6 depicts the pulsating current extracting performance using an HPF. The pulse frequency varies from 0.2–5 Hz, and the cutoff frequency for the HPF is 0.1 Hz. It is seen that it takes several pulse cycles to reach a steady state, during which the capacitor charging current signal is not sufficient to charge the capacitor to its designed upper limit. If the pulse frequency is constantly varying, which is always the case in the rocket launching application, the HPF method will result in a wrong current reference. As a result, the performance of the active capacitor deteriorates, the battery is forced to discharge more current, the bus voltage drops severely, and the coordinating sizing for the HPSS eventually fails.

To address this issue, this article proposes a simple current reference extracting method, as shown in Fig. 7. It includes four main detection or control units, namely the pulse detection unit, the regenerative energy detection unit, and the storage capacitor C_s charging and discharging control units. For the pulse detection unit, it is achieved by comparing the load current with a set current threshold of $I_{\mathrm{th}} = (I_n + I_p)/2$. Then, regenerative energy detection is simply realized by detecting the load current's direction. In addition, the charging and discharging control of the storage capacitor is justified according to the system's working conditions. On the one hand, it is discharging on condition that the load current is at pulse peak and the capacitor voltage is greater than its lowest allowable value. On the other hand, it should be charged when its voltage is less than the maximum allowable value. Importantly, it should be noted

Authorized licensed use limited to: CHONGQING UNIVERSITY. Downloaded on March 07,2026 at 09:05:34 UTC from IEEE Xplore. Restrictions apply.

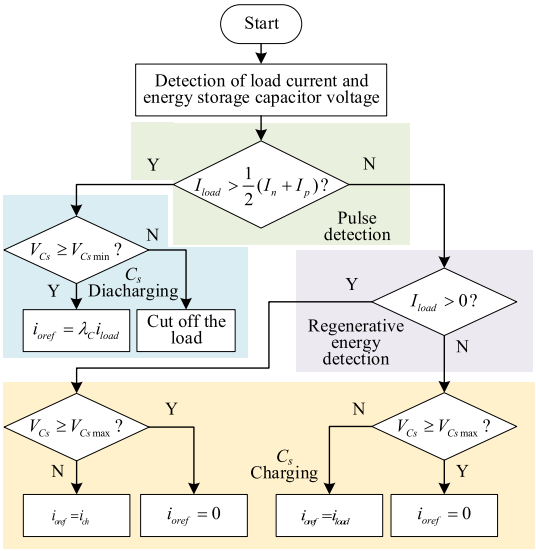

Fig. 7. Current reference generation logic.

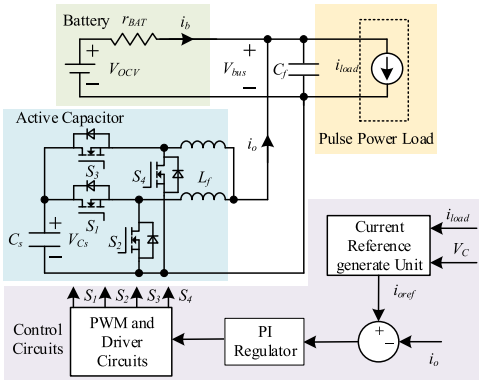

Fig. 8. Control system for active capacitor converter.

that in the discharging period of the storage capacitor (C_s), the coordinating sizing result is counted in the current reference generation. Specifically, the peak pulse current is multiplied by the optimum λ_C, as shown in Fig. 7.

Hence, after combining the proposed reference current extracting method with the control method proposed in [21], the control system of the PPSS is obtained, as shown in Fig. 8.

V. Case Study and Experimental Results

A. Case Analysis

A valve adjustment system of a rocket is considered in this case study. Its load profile, i.e., its required power, is depicted in Fig. 3. The system runs for a total time of 300 s, in which there are 320 pulses. The average pulse width is 40 ms.

In the volume calculations in this case study, a lithium battery cell type ASR00050 from Mouser is adopted as the main power supply calculation base. Similarly, an aluminum electrolytic capacitor type MAL250059102E3 from Vishay is used as the calculation base for the storage capacitor. For your comprehension, different main power supply ratings and storage capacitor ratings are formed by series and parallel connections of the calculation bases. According to the datasheet, the energy density of the ASR00050 battery cell is about 450 Wh/dm^3, that is, $k_{\mathrm{BAT}} \approx 1/450$, and according to (9), we can get $k_r \approx 0.02$. The relationship between the capacity of the capacitor MAL 250059102E3 and the volume is 0.00286 F/dm^3, that is, $k_c \approx 350$. Eventually, $\mathrm{Vol}_{\mathrm{CTRL}}$ is estimated as 1.26 L.

From the load characteristics shown in Fig. 3, it is observed that the minimum time interval between two pulses is 0.25 s. After deducting the pulse time of 0.04 s and energy regeneration time of 0.03 s, the minimum charging time t_{ch} is obtained as 0.18 s. It means that the storage capacitor must be charged to its nominal value in less than 0.18 s to maintain regular system operation.

Based on the coordinate sizing method proposed in Section II, it is calculated that $Q_{\mathrm{BAT1}} = 1.35$ Ah, $Q_{\mathrm{BAT2}}|_{\lambda C\,=\,0} = 21.6$ Ah, $Q_{\mathrm{BAT3}}|_{\lambda C\,=\,1} = 5.65$ Ah, the calculated battery capacity at the cross-point of Q_{BAT2} and Q_{BAT3} is 4.75 Ah, and $\lambda_C = 0.78$. This result is the same as Fig. 5(d). Therefore, to minimize the system volume, the desired power distribution mechanism is the battery supplying the constant load power and 22% of the pulsating power, while the active capacitor provides 78% of the pulsating load power. Therefore, according to (8), we can calculate that a 13.7 mF storage capacitor is required, so the total volume of the system is 8.91 L and the power-to-volume ratio is about 3.64 kW/L.

B. Comparisons With Other Solutions

For pulse PSSs that use batteries as the main supply, there are traditionally two schemes, the first is battery-only power supply and the second is hybrid battery-capacitor power supply. In [9], the authors employed NiCd batteries to power an electromechanical actuator (EMA) with a peak power of 35 kW on the X-38 Crew Return Vehicle, with a total battery volume of 45 L and a power-to-volume ratio of 0.78 kW/L. In [10], the authors employed lithium-ion batteries to power an EMA with a peak power of 50 kW on the P80 solid rocket motor (the first stage motor of the Vega rocket), and the power-to-volume ratio is about 2.16 kW/L. Similarly, the China Academy of Launch Vehicle Technology (CASVT) has studied this option in the past, and due to advances in battery technology, the power-to-volume ratio of this option has reached 2.5 kW/L.

In [7], [8], [21], and [22], the authors have employed active capacitors to absorb a portion of the pulsed power, which provides 100% pulsed power in [7] and [8], and 85% of the pulsed power in [21] and [22], but the effect of the distribution of the pulsed power between the active capacitors and the mains power supply as a percentage on the volume of the system has not been investigated. We find that the volume of the system is not optimal when the power distribution conclusions of [7], [8] or [21], [22] are used, and the calculation results are shown in Table I. According to Section V-A, under the load characteristic conditions shown in Fig. 5, the volumetrically optimal power distribution relationship is 22% of the pulsed power provided

Authorized licensed use limited to: CHONGQING UNIVERSITY. Downloaded on March 07,2026 at 09:05:34 UTC from IEEE Xplore. Restrictions apply.

TABLE I
COMPARISONS AMONG DIFFERENT POWER SUPPLY SCHEMES

Schemes	Industrial applications or academic research	Power-to-volume ratio
Battery-only	X-38 Crew Return Vehicle	0.78kW/L
	P80 solid rocket motor	2.16kW/L
	CASVT	2.5kW/L
Batteries with active capacitors	[7], [8]	3kW/L
	[21], [22]	3.44kW/L
	Our research	3.64kW/L

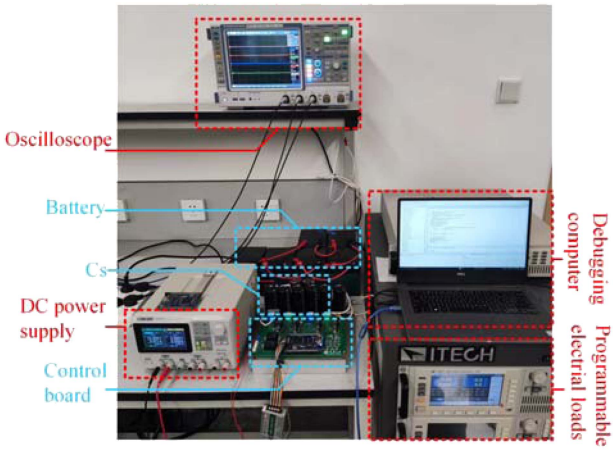

Fig. 9. Experiment platform.

by the battery and 78% of the pulsed power provided by the active capacitor, at which time the power-to-volume ratio of the system is 3.64 kW/L, which is a 45.6% improvement compared to the battery-only scheme, and a 21.3% and 5.8% improvement compared to [7], [8] and [21], [22], respectively.

C. Design of the Filter Inductor and Capacitor

According to [19] and the topology of the interleaving buck converter in Fig. 10, the filter inductor can be calculated as

$$L_f = \frac{(V_{Cs}(t) - V_{\text{bus}})V_{\text{bus}}}{f_s\left(\frac{\lambda_C I_p}{2} \times 20\%\right) V_{Cs}(t)} \tag{19}$$

where V_{Cs}(t) ranges from $V_{Cs\min}$–$V_{Cs\max}$, and f_s is the switching frequency. According to Table I, L_f is calculated as133 μH.

During loading of the pulse load, i_o takes some time t_r to reach its designed value, which can be expressed as

$$t_r = \frac{L_f \lambda_C I_P}{V_{Cs\max} - V_{\text{bus}}}. \tag{20}$$

Taking the parameter values into (20), we have $t_r = 27$ μs.

The product of R_{esr} and C_f equals 60 μs for a typical electrolytic capacitor, which is larger than t_r (=27 μs), so the maximum output voltage drop during the pulse cycle is

$$\Delta V_{\text{bus}} = I_p R_{\text{esr}}. \tag{21}$$

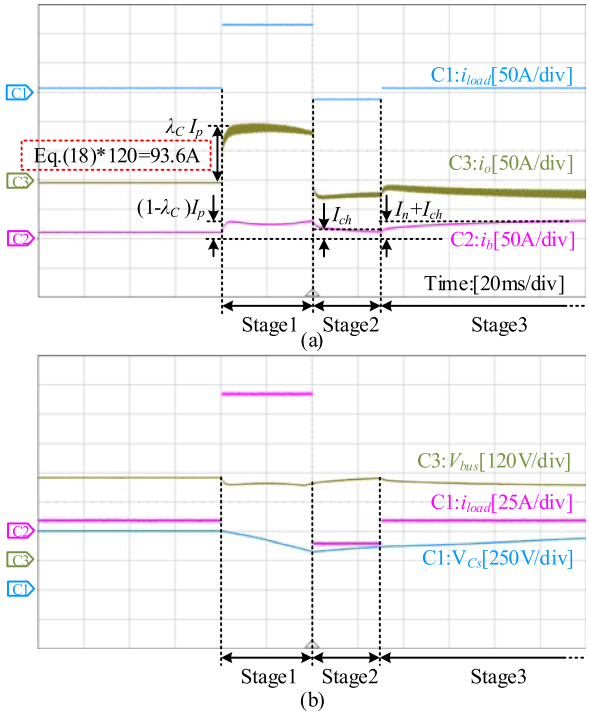

Fig. 10. Experimental results of the system with 0.2 Hz pulsating frequency.

TABLE II
SYSTEM PARAMETERS

Parameter	Value
Battery's nominal voltage V_{BAT}	270 V
Battery's capacity Q_{BAT}	4.75 Ah
Bus voltage V_{bus}	270 V
Storage capacitor C_s	13.7mF/600V
The variation range of storage capacitor's voltage V_{Cs}	320V-500V
Bus filter capacitor C_f	270μF/350V
Bidirectional dc/dc converter's inductor L_f	133μH
Switching frequency f_s	100kHz

Considering $\Delta V_{\text{bus}} = 270 \times 10\%$ and $I_p = 120$ A, the maximum allowed ESR can be calculated as 225 mΩ, therefore, a 270 μF C_f is chosen.

D. Experimental Results

A test-rig setup, which is shown in Fig. 9, is built in the lab to verify the validity of the coordinate sizing and control method for the PPSS. The system structure is the same as Fig. 9, where each power switch is composed of two parallel SiC MOSFETs (IPP65R045C7). The system parameters are detailed in Table II.

Fig. 10 shows the test results when the PPSS supplies power to a pulsed load with a pulsating frequency of 0.2 Hz. As can be seen in Fig. 10, the key operating waveforms of the PSS are the same as the ones we analyzed in Fig. 4; in the first stage, the battery and the active capacitor supply the pulsed load together, where the battery provides 78% of the pulsed power and the

Authorized licensed use limited to: CHONGQING UNIVERSITY. Downloaded on March 07,2026 at 09:05:34 UTC from IEEE Xplore. Restrictions apply.

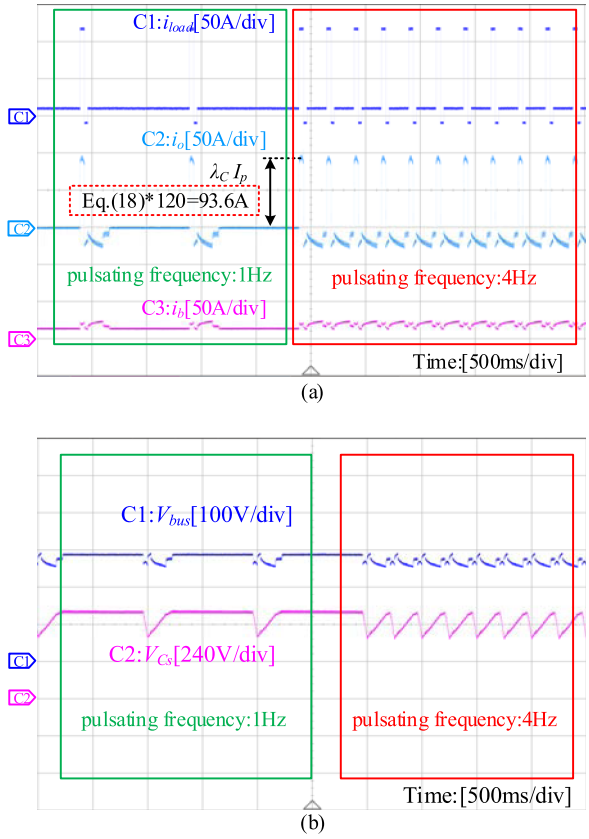

Fig. 11. Experimental results with pulsating frequencies varying from 1 to 4 Hz.

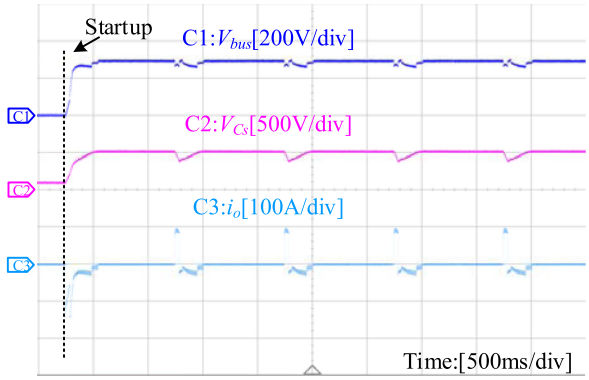

Fig. 12. Experimental results of the PPSS during startup.

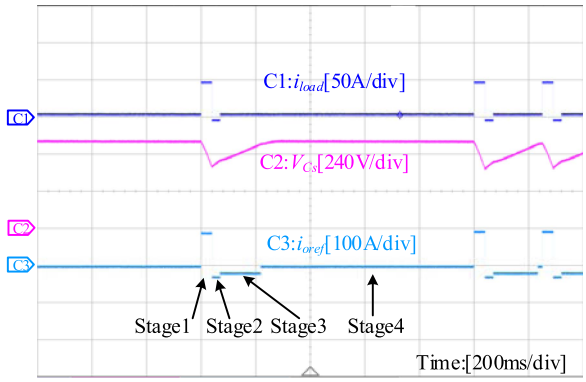

Fig. 13. Experimental results of the proposed current reference generation logic.

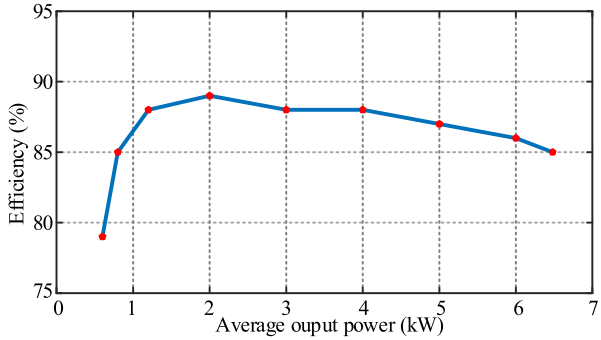

Fig. 14. Efficiency of the converter.

cell provides 22% of the pulsed power, which is consistent with the results we obtained in V-A; in the second stage, the active capacitor absorbs all of the regenerative energy and the battery simultaneously charges the active capacitor in this stage; and in the third stage, the battery supplies the constant load and simultaneously charges the *Cs* until it reaches the maximum voltage it was designed to operate at. During the whole working process, the bus voltage is maintained within the acceptable range (≥240 V), as can be seen in Fig. 10(b). Therefore, the system's good operation can be guaranteed with the proposed sizing and control method.

Fig. 11(a) provides the PPSS's performances when the pulsating frequency changes from 1 to 4 Hz. It is observed that the system is well performed during the whole process, and the pulsed power is also distributed in a way that matches our results in Section V-A. In addition, Fig. 11(b) shows the variations of the bus voltage and capacitor voltage at 1 and 4 Hz pulsating frequencies, respectively. The pulse loading frequency of 4 Hz is the limiting state of the system operation, and it can be seen from Fig. 11(b) that Stage 4 will cease to exist when the pulse frequency is 4 Hz, i.e., when C_s reaches its maximum design voltage, the next pulse load is immediately loaded, and under such a condition, it can be found that the bus voltage is maintained within the allowable range (≥240 V) throughout the whole operating period. Thus, the effectiveness of the proposed sizing method is verified.

Fig. 12 provides the startup waveform of the PPSS. It is observed that the energy storage capacitor C_s is rapidly charged during the startup, after which the bus voltage rises to its normal value. Fig. 13 provides the current reference signal which is determined by the load current and the voltage of the energy storage capacitor. It can be clearly seen that the generated current reference signal corresponds to Fig. 4 and is consistent with the current reference generation logic proposed in Fig. 7.

Fig. 14 provides the measured conversion efficiency of the converter. Compared with the passive decoupling scheme, the

Authorized licensed use limited to: CHONGQING UNIVERSITY. Downloaded on March 07,2026 at 09:05:34 UTC from IEEE Xplore. Restrictions apply.

active decoupling scheme increases the loss of the system, but the power density is greatly improved.

VI. Conclusion

This article proposes a coordinate sizing method considering distribution manner of the pulsed power between the main power supply and the active capacitor, which is easy to implement. We may make full use of the performance of each power supply unit by making the battery supply a small portion of the pulsating load power. As a result, the battery capacity and the storage capacitor can both be optimized, with a significant reduction in the total system volume and increased power density. Then, a simple pulse current extracting method for PPSS is proposed to improve the performance of the active capacitor under low and variable frequency. With the sizing mechanism and the control improvement, the PPSS's performance is proved to be improved by experiments.

Appendix

Based on (10) and (12), the values of Q_{BAT2} at $\lambda_C = 0$ and 1, and the value of Q_{BAT3} at $\lambda_C = 1$ are obtained as

$$Q_{\mathrm{BAT2}}|_{\lambda_C=0} = \frac{k_r V_{\mathrm{BAT}}(I_n + I_p)}{V_{\mathrm{BAT}} - V_{\mathrm{bus\,min}}} \tag{A1}$$

$$Q_{\mathrm{BAT2}}|_{\lambda_C=1} = \frac{k_r V_{\mathrm{BAT}} I_n}{V_{\mathrm{BAT}} - V_{\mathrm{bus\,min}}} \tag{A2}$$

$$Q_{\mathrm{BAT3}}|_{\lambda_C=1} = \frac{(I_p t_p - I_f t_f + I_n t_{\mathrm{ch}}) k_r V_{\mathrm{BAT}}}{t_{\mathrm{ch}}(V_{\mathrm{BAT}} - V_{\mathrm{bus\,min}})}. \tag{A3}$$

In order to ensure the normal operation of the system, the minimum voltage $V_{C\mathrm{min}}$ of capacitor C_s should be greater than the bus voltage V_{bus}. From (A1) and (A3), the relationship between Q_{BAT2} at $\lambda_C = 0$ and Q_{BAT3} at $\lambda_C = 1$ can be deduced as

$$\begin{aligned} &Q_{\mathrm{BAT2}}|_{\lambda_C=0} \geq Q_{\mathrm{BAT3}}|_{\lambda_C=1} \\ &\Leftrightarrow I_p t_{\mathrm{ch}} > I_p t_p. \end{aligned} \tag{A4}$$

Since Q_{BAT3} is monotonically increasing, the value of Q_{BAT2} at $\lambda_C = 0$ is also greater than the value of Q_{BAT3} at $\lambda_C = 0$.

According to the load profile shown in Fig. 3, the regenerative energy is generally lower than 30% of the pulse energy. Combining (A2) and (A3), the relationship between Q_{BAT3} at $\lambda_C = 1$ and Q_{BAT2} at $\lambda_C = 1$ can be deduced as

$$\begin{aligned} &Q_{\mathrm{BAT3}}|_{\lambda_C=1} \geq Q_{\mathrm{BAT2}}|_{\lambda_C=1} \\ &\Leftrightarrow I_p t_p > I_f t_f. \end{aligned} \tag{A5}$$

Therefore, the relationship between Q_{BAT} and λ_C can be determined, as shown in Fig. 5.

References

[1] B. Sarlioglu and C. T. Morris, "More electric aircraft: Review, challenges, and opportunities for commercial transport aircraft," *IEEE Trans. Transp. Electrific.*, vol. 1, no. 1, pp. 54–64, Jun. 2015.

[2] V. Madonna, P. Giangrande, and M. Galea, "Electrical power generation in aircraft: Review, challenges, and opportunities," *IEEE Trans. Transp. Electrific.*, vol. 4, no. 3, pp. 646–659, Sep. 2018.

[3] E. Sayed et al., "Review of electric machines in more-/hybrid-/turbo-electric aircraft," *IEEE Trans. Transp. Electrific.*, vol. 7, no. 4, pp. 2976–3005, Dec. 2021.

[4] K. Ni, Y. Hu, Z. Wang, H. Wen, and C. Gan, "Asynchronized synchronous motor-based more electric ship—Less power electronics for more system reliability," *IEEE/ASME Trans. Mechatron.*, vol. 24, no. 5, pp. 2353–2364, Oct. 2019.

[5] Z. Jin, L. Meng, J. M. Guerrero, and R. Han, "Hierarchical control design for a shipboard power system with DC distribution and energy storage aboard future more-electric ships," *IEEE Trans. Ind. Inform.*, vol. 14, no. 2, pp. 703–714, Feb. 2018.

[6] K. Hein, Y. Xu, G. Wilson, and A. K. Gupta, "Coordinated optimal voyage planning and energy management of all-electric ship with hybrid energy storage system," *IEEE Trans. Power Syst.*, vol. 36, no. 3, pp. 2355–2365, May 2021.

[7] J. Chen, H. Wu, J. Zhu, L. Li, and Y. Xing, "A three-phase AC/DC power system with paralleled active and passive rectifiers for low-frequency pulsed load applications," in *Proc. IEEE 9th Int. Power Electron. Motion Control Conf.*, 2020, pp. 1595–1599.

[8] X. Gao, H. Wu, S. Gao, Z. Zhang, and Y. Xing, "A two-stage pulsed power supply for low-dc-voltage and low-frequency pulsed-current loads," *IEEE Trans. Power Electron.*, vol. 36, no. 2, pp. 2298–2309, Feb. 2021.

[9] E. Darcy, F. Davies, L. Hummer, and B. Strangways, "270V Battery using COTS NiCd cells for manned spacecraft," in *Proc. 40th Power Sources Conf.*, 2002, pp. 1–4.

[10] T. Vanthuyne, "An electrical thrust vector control system for the VEGA launcher," in *Proc. 13th Eur. Space Mech. Tribol. Symp.*, 2009, pp. 1–7.

[11] "2022 VTO annual merit review results report – ELECTRIFICATION," VTO, 2022. [Online]. Available: https://www.energy.gov/sites/default/files/2022-12/04_Electrification.pdf

[12] H. Zheng, W. Wu, and Y. Wang, "Integrated motion and powertrain predictive control of intelligent fuel cell/battery hybrid vehicles," *IEEE Trans. Ind. Inform.*, vol. 16, no. 5, pp. 3397–3406, May 2020.

[13] A. Ferrara and C. Hametner, "Impact of energy management strategies on hydrogen consumption and start-up/shut-down cycles in fuel cell-ultracapacitor-battery vehicles," *IEEE Trans. Veh. Technol.*, vol. 71, no. 6, pp. 5692–5703, Jun. 2022.

[14] L. Zhou, W. Yi, and Y. Chen, "Additional synchronous torque coordinated control for approximate-capacity diesel-storage supply system with low-frequency pulsed load," *IEEE Trans. Ind. Electron.*, vol. 70, no. 7, pp. 6919–6930, Jul. 2023.

[15] L. Zhou et al., "High overload power supply system and its energy synchronization control method for short-term high-energy pulse load," *IEEE Trans. Smart Grid*, vol. 13, no. 2, pp. 849–860, Mar. 2022.

[16] J. M. Crider and S. D. Sudhoff, "Reducing impact of pulsed power loads on microgrid power systems," *IEEE Trans. Smart Grid*, vol. 1, no. 3, pp. 270–277, Dec. 2010.

[17] M. T. Penella and M. Gasulla, "Runtime extension of low-power wireless sensor nodes using hybrid-storage units," *IEEE Trans. Instrum. Meas.*, vol. 59, no. 4, pp. 857–865, Apr. 2010.

[18] M. M. Mardani, M. H. Khooban, A. Masoudian, and T. Dragičević, "Model predictive control of dc–dc converters to mitigate the effects of pulsed power loads in naval dc microgrids," *IEEE Trans. Ind. Electron.*, vol. 66, no. 7, pp. 5676–5685, Jul. 2019.

[19] Y. Yao, G. S. Kulothungan, H. S. Krishnamoorthy, A. Das, and H. Soni, "GaN-based two-stage converter with high power density and fast response for pulsed load applications," *IEEE Trans. Ind. Electron.*, vol. 69, no. 10, pp. 10035–10044, Oct. 2022.

[20] Y. Gu, D. Zhang, M. Fang, X. Zhang, and P. Qi, "Research on low input current ripple two-stage converter for low frequency pulsed-power applications," *IET Power Electron.*, vol. 13, no. 2, pp. 340–345, 2020.

[21] X. Huang, X. Ruan, F. Du, L. Fei, and Z. Li, "A pulsed power supply adopting active capacitor converter for low-voltage and low-frequency pulsed loads," *IEEE Trans. Power Electron.*, vol. 33, no. 11, pp. 9219–9230, Nov. 2018.

[22] X. Huang, X. Ruan, F. Du, L. Fei, and Z. Li, "High power and low voltage power supply for low frequency pulsed load," in *Proc. IEEE Appl. Power Electron. Conf. Expo.*, 2017, pp. 2859–2865.

[23] P. Yang, X. Chen, R. Chen, Y. Peng, and J. Xu, "Stability improvement of pulse power supply with dual-inductance active storage unit using hysteresis current control," *IEEE J. Emerg. Sel. Topics Circuits Syst.*, vol. 11, no. 1, pp. 111–120, Mar. 2021.

Authorized licensed use limited to: CHONGQING UNIVERSITY. Downloaded on March 07,2026 at 09:05:34 UTC from IEEE Xplore. Restrictions apply.

[24] P. Yang et al., "A three-state dual-inductance bi-directional converter and its control in pulse-loaded three-port converters," *CSEE J. Power Energy Syst.*, vol. 6, no. 2, pp. 291–297, 2020.
[25] J. Sanchez, D. Wetz, Q. Dong, and J. Heinzel, "Integration and study of hardware in the loop diesel generator with a hybrid energy storage module for naval applications," in *Proc. IEEE Electric Ship Technol. Symp.*, 2017, pp. 580–585.
[26] M. S. Wasim, S. Habib, M. Amjad, A. R. Bhatti, E. M. Ahmed, and M. A. Qureshi, "Battery-ultracapacitor hybrid energy storage system to increase Battery life under pulse loads," *IEEE Access*, vol. 10, pp. 62173–62182, 2022.
[27] F. Ai, J. Zhang, Y. Qi, W. Li, and J. Deng, "More electrical aircraft pulsed power mitigation through active capacitor converter," in *Proc. CSAA/IET Int. Conf. Aircr. Utility Syst.*, 2022, pp. 1301–1306.
[28] A. Abbassi, M. A. Dami, and M. Jemli, "A statistical approach for hybrid energy storage system sizing based on capacity distributions in an autonomous PV/wind power generation system," *Renewable Energy*, vol. 103, pp. 81–93, 2017.
[29] T. Mesbahi, F. Khenfri, N. Rizoug, P. Bartholomeüs, and P. L. Moigne, "Combined optimal sizing and control of li-ion battery/supercapacitor embedded power supply using hybrid particle swarm–Nelder–Mead algorithm," *IEEE Trans. Sustain. Energy*, vol. 8, no. 1, pp. 59–73, Jan. 2017.
[30] P. Li, D. Xu, Z. Zhou, W. J. Lee, and Z. Bo, "Stochastic optimal operation of microgrid based on chaotic binary particle swarm optimization," *IEEE Trans. Smart Grid*, vol. 7, no. 1, pp. 66–73, Jan. 2016.
[31] P. Xie, Z. Cai, P. Liu, X. Li, Y. Zhang, and D. Xu, "Microgrid system energy storage capacity optimization considering multiple time scale uncertainty coupling," *IEEE Trans. Smart Grid*, vol. 10, no. 5, pp. 5234–5245, Sep. 2019.
[32] M. Alramlawi and P. Li, "Design optimization of a residential PV-battery microgrid with a detailed battery lifetime estimation model," *IEEE Trans. Ind. Appl.*, vol. 56, no. 2, pp. 2020–2030, Mar./Apr. 2020.
[33] N. Y. Soltani and A. Nasiri, "Chance-constrained optimization of energy storage capacity for microgrids," *IEEE Trans Smart Grid*, vol. 11, no. 4, pp. 2760–2770, Jul. 2020.
[34] O. Tremblay, L. A. Dessaint, and A. I. Dekkiche, "A generic battery model for the dynamic simulation of hybrid electric vehicles," in *Proc. IEEE Veh. Power Propulsion Conf.*, 2007, pp. 284–289.



Wenjie Ao (Graduate Student Member, IEEE) was born in Chongqing, China, in 1996. He received the B.S. degree in automation from the Southeast University, Nanjing, China, in June 2019. He is currently working toward the Ph.D. degree in control theory and control engineering with the School of Automation, Chongqing University, Chongqing, China.

His research interests include pulsed power supply for electrified vehicles, and capacity optimization configuration.



Jiawei Chen (Senior Member, IEEE) received the B.S. and Ph.D. degrees in electrical engineering from the Nanjing University of Aeronautics and Astronautics, Nanjing, China, in 2008 and 2013, respectively.

From October 2013 to August 2015, he worked as a Research Fellow with the Rolls Royce @ NTU Co-lab, Singapore, doing research on the intelligent energy management system for future more electric aircraft. Later, he joined the Chongqing University, Chongqing, China, where he is currently a Full Professor. His research interests include renewable energy generation systems, power control and energy management strategies for distributed energy generation systems and micro-grids, and the power electronics circuits in these systems.

Prof. Chen is an Associate Editor for the IEEE TRANSACTIONS ON INDUSTRIAL ELECTRONICS AND CONTROL AND DECISION.

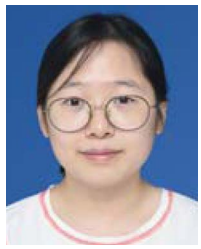

Wenjie Lv received the bachelor's degree in automation from the Chongqing University, Chongqing, China, in 2022. She is currently working toward the master's degree in electonic engineering with the Chongqing University, Chongqing, China.

Her research interests include renewable energy generation systems, power control, and embedded system development.

Authorized licensed use limited to: CHONGQING UNIVERSITY. Downloaded on March 07,2026 at 09:05:34 UTC from IEEE Xplore. Restrictions apply.